Efficient capture of trace acetylene by an ultramicroporous metal–organic framework with purine binding sites

Efficient Capture of Trace Acetylene by an Ultramicroporous Metal–Organic Framework with Purine Binding Sites

Shivani Sharma,[⊥] Soumya Mukherjee,[⊥] Aamod V. Desai, Matthias Vandichel, Gourab K. Dam, Ashwini Jadhav, Gabriele Kociok-Köhn, Michael J. Zaworotko,* and Sujit K. Ghosh*

Cite This: *Chem. Mater.* 2021, 33, 5800–5808

ABSTRACT: Efficient separation of acetylene (C_2H_2) from its byproducts, especially CO_2, is difficult because of their similar physicochemical properties, including molecular dimensions and boiling point. Herein, we demonstrate trace C_2H_2 removal from C_2H_2/CO_2 mixtures enabled by a new ultramicroporous metal–organic framework (MOF) adsorbent, IPM-101, which features an optimal pore size of 4 Å (close to the kinetic diameter of C_2H_2, 3.3 Å) and one-dimensional channels lined by Lewis basic purine groups. Single-component gas adsorption isotherms revealed a clear affinity toward C_2H_2 versus CO_2 at low pressures with a substantial C_2H_2 uptake of 0.9 mmol g^{-1} at 3000 ppm and 298 K. Dynamic column breakthrough experiments revealed separation of C_2H_2 from 1:1 and 1:99 v/v C_2H_2/CO_2 mixtures. IPM-101 exhibits one of the highest dynamic separation selectivity (α_{AC}) values yet reported, 22.5 for 1:1 C_2H_2/CO_2. Computational simulations indicated that the purine moiety was key to the strong C_2H_2 selectivity thanks to C_2H_2 selective N···HC≡CH interactions.

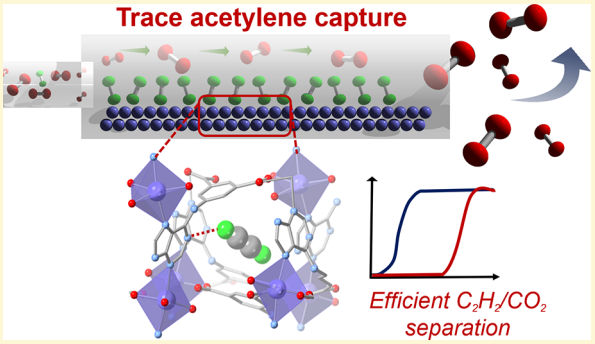

1. INTRODUCTION

Acetylene (C_2H_2) purification is one of the most challenging and energy-intensive chemical separations in the petrochemical industry.[1] Widely utilized as a raw material to produce important chemicals or as a fuel, pure C_2H_2 (>99% purity grade) is a key commodity with a projected market value of ~6.9 billion US$ by 2025.[2] Typically, C_2H_2 is produced via thermal cracking and then coexists with several byproducts, including carbon dioxide (CO_2) and methane (CH_4). Purification is required before commercial utilization[3,4] but the separation of C_2H_2 from CO_2 is a challenging task because of their similar physicochemical properties. For instance, C_2H_2 (3.18 × 3.33 × 5.36 $Å^3$) and CO_2 (3.32 × 3.34 × 5.7 $Å^3$) have comparable molecular dimensions, similar boiling points (ΔT ~ 5 K), and near-identical kinetic diameters (3.3 Å).[5] Further, C_2H_2 exhibits a dangerously low flammability limit (~2.5% concentration), rendering the removal of even trace amounts from gas streams challenging but necessary from a safety standpoint.[6] State-of-the-art methods employed in C_2H_2 purification/capture including cryogenic distillation and large-scale solvent separation are energy-intensive and environmentally damaging and lack selectivity.[7]

To address this challenge, researchers have studied adsorptive separation methods based on custom-designed porous solid adsorbents[8] as exemplified by metal–organic frameworks (MOFs)[9]/porous coordination polymers (PCPs).[10] MOFs offer potential for diverse applications including molecular sensing,[11,12] chemical separation,[13−15] catalysis,[16,17] pollutant capture,[18,19] and electrical or ionic conductivity.[20−22] The diversity of potential applications results from high surface area, modularity with respect to linker ligands and/or metal ions/clusters, and fine tunability of pore size/chemistry, which also set these MOFs apart from traditional porous adsorbents like zeolites, mesoporous silica, and porous carbons.[23−25] Moreover, the low energy footprint for regenerating physisorbents makes them excellent candidates for gas separations, especially in the context of gas purification-based downstream processes.[26,27] Thus far, MOFs and related materials such as hybrid ultramicroporous materials (HUMs),[28] have been examined for key industrial separations including CO_2/N_2,[29−33] C_2H_2/CO_2,[5,34] C_2H_2/C_2H_4,[35,36] C_2H_4/C_2H_6,[37−39] C_3H_4/C_3H_6,[40] and C_3H_6/C_3H_8.[41] For C_2H_2/CO_2 separation, insights from the literature suggest that pore surface functionality such as Lewis basic moieties (amines, polar oxygens, etc.),[3,42,43] inorganic anions (MF_6, M = Si, Ti, etc.),[5,44] or open metal sites[34,45−48] promote selective C_2H_2 binding through noncovalent interactions or coordina-

Received: May 19, 2021
Revised: June 23, 2021
Published: July 9, 2021

https://doi.org/10.1021/acs.chemmater.1c01723

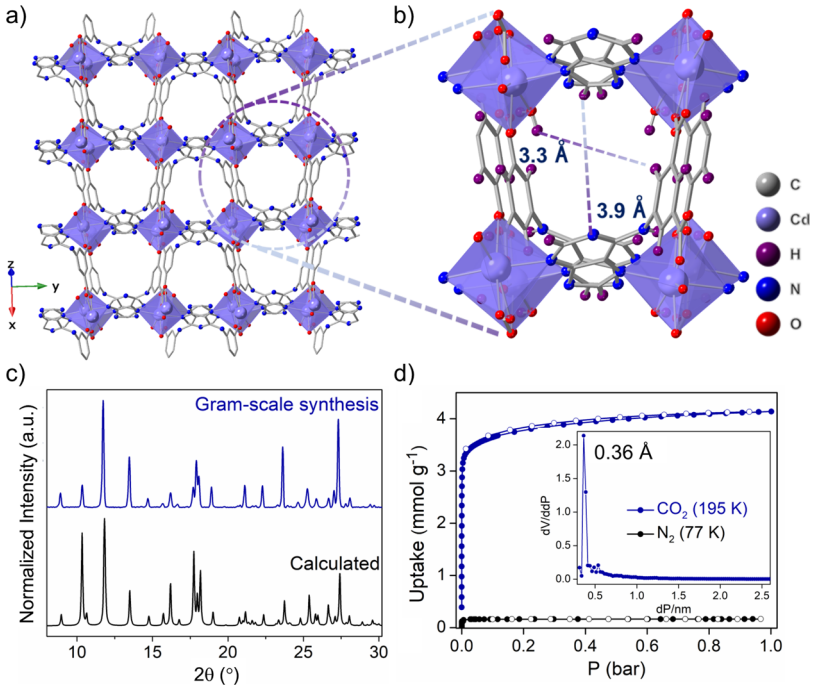

Figure 1. For IPM-101, (a) perspective view of the one-dimensional channels (guest solvent molecules and hydrogen atoms omitted for clarity); (b) zoomed view of a single ultramicroporous channel highlighting the calculated pore aperture (hydrogen atoms and van der Waals radii of atoms were included during the distance determination; solvent molecules omitted for clarity); (c) experimental validation of bulk phase purity based on the PXRD pattern of IPM-101 synthesized in gram scale; (d) single-component adsorption isotherms for activated IPM-101: N_2 at 77 K and CO_2 at 195 K. Inset: pore-size distribution analysis (Horvath−Kawazoe plot) of IPM-101.

tion bonds. MOFs can also invoke various supramolecular design approaches to enable C_2H_2/CO_2 separation, including the following: (a) electrostatic interactions,[49] (b) induced fit-mediated gate opening,[50,51] or a combination thereof.[52] Whereas the number of MOFs is now >100 000,[54] those that exhibit C_2H_2/CO_2 selectivity remain rare.[53,55] Moreover, MOFs that offer dynamic C_2H_2/CO_2 separation evidenced by conducting dynamic column breakthrough (DCB) experiments are even fewer (<20). This small group of C_2H_2 selective adsorbents tends to offer either selectivity or high uptake capacity, but not both. Further, another way to separate C_2H_2/CO_2 mixtures is to fabricate CO_2 selective sorbents; which is challenging owing to the highly polar nature of C_2H_2, and some of the noteworthy examples highlight this strategy.[56−59] With respect to C_2H_2/CO_2 separation, benchmark MOFs such as NKMOF-1-Ni[48] and ZJU-74a[34] exhibit high C_2H_2 affinity at low pressure aided by C_2H_2 binding pockets and tight pore dimensions with respect to C_2H_2, ultimately resulting in benchmark selectivity for C_2H_2. However, such high affinity in the low-pressure region does not necessarily translate into trace capture behavior (i.e., at 1:99 v/v) under dynamic conditions, with only MUF-17[60] and TCuX[61] (X = Cl, Br, I) having demonstrated trace C_2H_2 capture behavior from 1:99 C_2H_2/CO_2. These limited studies highlight the need for investigations that focus on the role of pore chemistry to enable trace C_2H_2 capture. Recent studies have revealed that adenine groups with multiple Lewis basic sites can enhance C_2H_2 affinity and result in efficient C_2H_2/C_2H_4 separations.[62,63] Inspired by these studies, we report herein a previously unreported ultramicroporous MOF, IPM-101 (IPM= IISER Pune Materials) $[\{Cd(L)(H_2O)\}\cdot(DMF)\text{-}(H_2O)]_n$ (wherein H_2L = 5-((9*H*-purin-6-yl)amino)isophthalic acid, G = guest solvent molecules H_2O and DMF (*N*,*N*-dimethylformamide)), based upon a new purine ligand and investigate its performance with respect to C_2H_2/CO_2 separation.

2. RESULTS AND DISCUSSION

IPM-101 was synthesized by solvothermally reacting ligand (L) and $Cd(NO_3)_2\cdot 4H_2O$ in a mixture of water/DMF/nitric acid, yielding block-shaped single crystals (Experimental Section, Schemes S1 and S2). Presence of nitric acid during crystallization was key to obtaining high-quality crystals suitable for single-crystal X-ray diffraction (SC-XRD) analysis. SC-XRD data revealed that IPM-101 crystallized in the monoclinic $P2_1/n$ space group (Table S1). The asymmetric unit of IPM-101 comprises one Cd(II) as the metal node, one ligand (L), one coordinated water molecule, and DMF/H_2O as guest molecules (Figure S2). Each Cd(II) ion adopted pentagonal bipyramidal geometry with the coordination sphere comprising one water molecule, four oxygen atoms, and two nitrogen atoms belonging to two carboxylate and purine moieties from four different linkers (Figure S3). Overall, the network exhibits **sra** topology with point group $\{4^2.6^3.8\}$ (Figure S5). The structure features one-dimensional porous channels with a pore dimension of ~3.3 × 3.9 Å^2 (Figures 1a,b, S4, and S6). Guest accessible void volume as estimated by PLATON[64] was found to be 515 Å^3, accounting for 26.1% of the unit cell volume. Bulk phase purity was confirmed by powder X-ray diffraction (PXRD) analysis (Figure S7) and the PXRD patterns of IPM-101 synthesized at gram scale as well as after soaking in various aromatic solvents match well with the calculated pattern (Figures 1c and S8). Thermogravimetric analysis (TGA) profile revealed weight loss corresponding to the guest molecules present in the pores (Figure S9).

https://doi.org/10.1021/acs.chemmater.1c01723

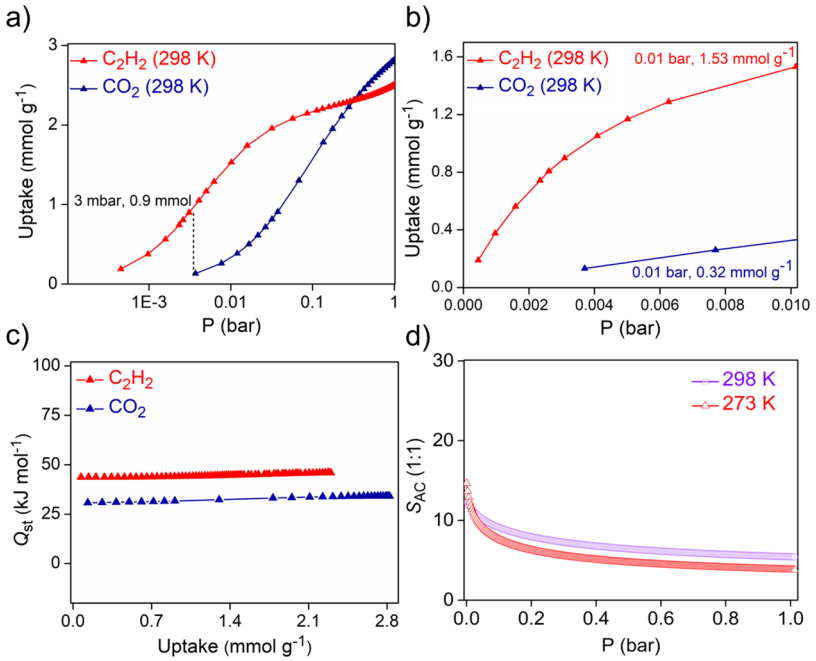

Figure 2. For IPM-101, (a, b) adsorption isotherms for CO_2 and C_2H_2 at 298 K: (a) logarithmic pressure axis scale, (b) zoomed view of the low-pressure range <0.01 bar; (c) Q_{st} plots of C_2H_2 and CO_2; (d) IAST selectivity for C_2H_2/CO_2 (1:1) binary mixture at 273 and 298 K.

The activated phase of IPM-101 was characterized by its PXRD pattern, which confirmed retention of crystallinity, phase purity, and the rigid nature of IPM-101 (Figure S7). Also, field emission scanning electron microscopy (FESEM) and elemental analysis confirmed retention of block shape morphology and composition, respectively (Figures S10 and S11). Fourier transform infrared spectroscopy (FT-IR) revealed peaks corresponding to ligand L (Figure S12). To investigate the permanent porosity of IPM-101, low-temperature gas adsorption measurements were performed including N_2 (77 K) and CO_2 (195 K). We observed negligible uptake for N_2 (77 K) as seen for some other ultramicroporous physisorbents (Figure 1d),[4,65] whereas CO_2 adsorption (195 K) showed a steep uptake (Type I adsorption isotherm) with a loading of ~4 mmol g^{-1} at 1 bar, confirming the microporosity (Figure 1d). Conforming to the Rouquerol criteria,[66] the Brunauer–Emmett–Teller (BET) surface area calculated from the CO_2 (195 K) isotherm was determined to be ~343 m^2 g^{-1}, comparable to some of the benchmark ultramicroporous MOFs studied for C_2H_2/CO_2 separation, including UTSA-300a (311 m^2 g^{-1}),[44] FeNi-M′MOF (383 m^2 g^{-1}),[67] NKMOF-1-Ni (380 m^2 g^{-1}),[48] and DICRO-4-Ni-i (398 m^2 g^{-1}).[68] Pore-size distribution analysis based on the Horvath–Kawazoe model (pore geometry: cylinder) for CO_2 (195 K) indicated a narrow pore aperture of ~3.6 Å that agrees well with the pore dimensions determined by SC-XRD analysis (3.3 × 3.9 $Å^2$) (Figure 1b,d (inset)).

We next investigated the adsorption properties of IPM-101 toward CO_2 and C_2/C_3 hydrocarbons. Single-component adsorption isotherms for N_2, CO_2, CH_4, C_2H_2, C_2H_4, C_2H_6, C_3H_4, C_3H_6, and C_3H_8 were recorded at 273 and 298 K up to 1 bar (Figures S13–S18). These pure gas adsorption isotherms revealed that IPM-101 adsorbs nearly 3.04 mmol g^{-1} of CO_2, 2.55 mmol g^{-1} of C_2H_2, 0.33 mmol g^{-1} of CH_4, 2.28 mmol g^{-1} of C_2H_4, 2.25 mmol g^{-1} of C_2H_6, 2.37 mmol g^{-1} of C_3H_4, 2.33 mmol g^{-1} of C_3H_6, and 2.29 mmol g^{-1} of C_3H_8 at 298 K, 1 bar (Figures S13–S16). Further, comparative inspection of the C_2H_2 and CO_2 sorption isotherms at 273 and 298 K revealed considerable difference in uptakes especially in the low-pressure region (Figures 2b and S17c). No such distinction was observed at 195 K with consistent uptakes of ~4.1 mmol g^{-1} (Figure S17a). Under ambient conditions, IPM-101 exhibited high affinity toward C_2H_2 at low pressures, resulting in an uptake of ~0.9 mmol g^{-1} at just 3000 ppm, i.e., 3 mbar (Figure 2a). Conversely, at the same pressure, CO_2 uptake was observed to be negligible, ~0.10 mmol g^{-1}.

Notably, such selectivity for C_2H_2/CO_2 separation in the low-pressure region (<10 000 ppm) has been exhibited by only a handful of physisorbents, including NKMOF-1-Ni (1.50 mmol g^{-1}),[48] NKMOF-1-Cu (1.15 mmol g^{-1}),[48] TIFSIX-2-Cu-i (1.10 mmol g^{-1}),[5] and DICRO-4-Ni-i (0.40 mmol g^{-1})[68] (Table S2). Also, at 0.01 bar, IPM-101 adsorbs 1.53 mmol g^{-1} of C_2H_2, comparable to the top-performing adsorbents including MUF-17 (1.4 mmol g^{-1}),[60] NKMOF-1-Ni (1.74 mmol g^{-1}),[48] TIFSIX-2-Cu-i (1.78 mmol g^{-1}),[5] and UTSA-200a (1.83 mmol g^{-1})[69] (Figure 2b and Table S2). Comparison of the C_2H_2 and CH_4 adsorption profiles for IPM-101 indicated a strong affinity toward C_2H_2 as there was negligible uptake for CH_4 at 273 and 298 K (Figure S18). The isosteric heats of adsorption, Q_{st}, for C_2H_2, CO_2, and CH_4 were determined from their respective adsorption isotherms (Figures 2a, S16, and S17) by fitting them to a virial-type expression (Methods Section in the SI, Figures S24–S26, Table S3). The low-coverage Q_{st} values for C_2H_2, CO_2, and CH_4: $Q_{st}(C_2H_2)$, $Q_{st}(CO_2)$, and $Q_{st}(CH_4)$, were determined to be 43.7, 30.7, and 22.7 kJ mol^{-1}, respectively (Figures 2c and S19).

The significantly higher Q_{st} for C_2H_2 over CO_2 and CH_4 explains the affinity for C_2H_2 by IPM-101. Additionally, the $Q_{st}(C_2H_2)$ profile remains consistent from low pressure until 1 bar, indicating a single type of binding site to facilitate physisorption (Figure 2c). Notably, the low-loading $Q_{st}(C_2H_2)$ ~ 43.7 kJ mol^{-1} for IPM-101 surpasses several benchmark C_2H_2 selective physisorbents, including DICRO-4-Ni-i (37.7

https://doi.org/10.1021/acs.chemmater.1c01723

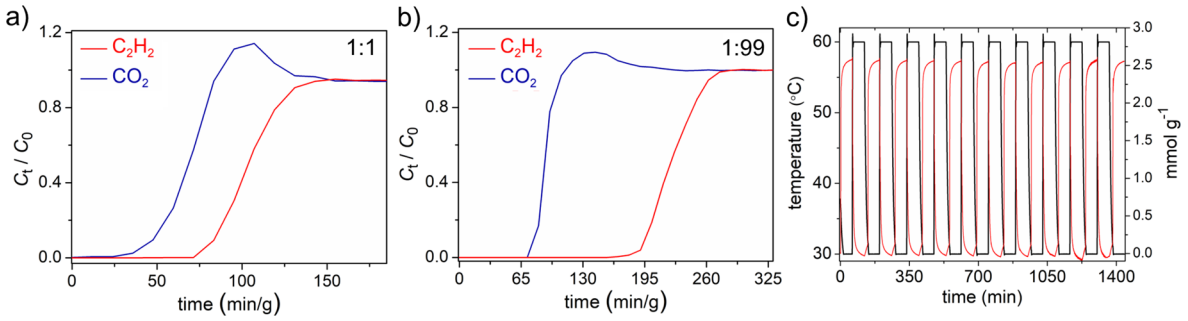

Figure 3. For IPM-101 packed bed, experimental DCB curves recorded for C_2H_2/CO_2 mixtures (a) 1:1, (b) 1:99 compositions at 298 K and 1 bar. (c) C_2H_2 sorption recycling data (IPM-101 regeneration was conducted at 60 °C under N_2 flow of 20 cm^3 min^{-1}).

kJ mol^{-1}),[68] UTSA-74a (31 kJ mol^{-1}),[46] FeNi-M′MOF (27 kJ mol^{-1}),[67] and TCuCl (37.7)[61] (Table S2). This enthalpy data highlights the performance of IPM-101 with respect to the thermodynamics of C_2H_2 capture; however, favorable sorption kinetics is also a key to sorbent performance.[70] Analysis of the relative sorption kinetics indicates higher affinity of IPM-101 toward C_2H_2 with a significant uptake of ∼1.5 mmol g^{-1} (∼60% of the equilibrium C_2H_2 adsorption capacity at 298 K) within 5 min, as opposed to an almost negligible uptake for CO_2 (Figure S20). Overall, IPM-101 exhibited favorable sorption thermodynamics and kinetics for C_2H_2 versus CO_2, motivating us to further evaluate its adsorption selectivity. The ideal adsorbed solution theory (IAST) was employed to determine the adsorption selectivity of IPM-101 for various gas mixtures, including C_2H_2/CO_2 (1:1), C_2H_2/CH_4 (1:1), and C_2H_2/CO_2 (1:99) (Figures 2d and S21).

C_2H_2/CO_2 selectivity (S_{AC}) was calculated to be ∼14.7 and ∼12.3 for an equimolar mixture (v/v) at 273 and 298 K, respectively, at low pressures (Figure 2d). The selectivity of ∼12.3 at low pressure drops to ∼5.4 at 1 bar, comparable to the previously reported top-performing adsorbents TIFSIX-2-Cu-i (6.5),[5] UTSA-74a (9),[46] and MUF-17 (6),[60] but lower than materials such as UTSA-300a (743),[44] ZJU-74a (36), FeNi-M′MOF (24), NKMOF-1-Ni (22), HOF-3a (21), and DICRO-4-Ni-I (18.2) (values in the parentheses reflect the S_{AC} at 1 bar, 298 K). Additionally, IPM-101 shows trace (1:99) selectivity of 5.3 for C_2H_2/CO_2 at 1 bar, which is even higher at lower pressures, e.g., at 3000 ppm, S_{AC} is ca. 10.5 (Figure S21a). These IAST selectivities are comparable to the best-performing adsorbents in the current C_2H_2/CO_2 separation literature.[53] We also estimated the selectivity for an equimolar mixture of C_2H_2/CH_4, S_{AM}, which was found to be ∼2.0 × 10^4 and ∼2.3 × 10^4 at 273 and 298 K, respectively, at the saturation pressure of 1 bar (Figure S21b). These record-high selectivities endow IPM-101 as the current benchmark in the literature of MOFs for C_2H_2/CH_4 separation when compared to ZJU-74a (∼1.5 × 10^4),[34] NKMOF-1-Ni (6409.1),[48] ZJU-198a (391.1),[71] and Cu-TDPAH (127.1).[72] This motivated us to probe the separation performance of IPM-101 toward C_2H_2/CO_2 mixtures through real-time dynamic column breakthrough (DCB) studies. DCB experiments were performed with a fixed bed packed with activated IPM-101, and C_2H_2/CO_2 mixture streams were fed at two different ratios, i.e., 1:1 and 1:99 (v/v) under ambient conditions (Figure S27). For the equimolar mixture of C_2H_2/CO_2 (1:1), separation was observed with CO_2 elution occurring at 23 min g^{-1} with an effluent purity of >99.967%, while for C_2H_2, breakthrough occurred at 71 min g^{-1} (Figure 3a). From the equimolar DCB experiment, C_2H_2 saturation uptake was estimated as 1.52 mmol g^{-1}, lower than the single-component uptake at half-loading (∼2.4 mmol g^{-1}, Figure 2a), in part accounted to the experimentally determined dead volume of our DCB setup (see Methods Section in the SI).

The dynamic separation selectivity (α_{AC}), a metric that reflects the dynamic mixture separation performance of adsorbents, was determined to be ∼22.5 for the C_2H_2/CO_2 (1:1) mixture. α_{AC} for IPM-101 with a value of 22.5 is higher than a number of leading C_2H_2 selective physisorbents, namely, UTSA-74a (20.1),[46] ZJU-74a (4.3),[46] NKMOF-1-Ni (2.6),[48] and HOF-3a (2.0),[73] but below that of the TCuX platform (33.4, 104.5, 143.1 for X = I, Br, Cl, respectively)[61] and sql-16-Cu-NO_3-α' (78).[74] The performance of IPM-101 for trace acetylene capture from a binary mixture 1:99 (v/v) revealed the capture of C_2H_2 from this diluted mixture as well (Figure 3b). Notably, CO_2 eluted from the IPM-101 adsorbent bed contained negligible amounts of C_2H_2 (∼1227.3 ppm) and a high effluent purity of ∼99.88%, better than the commercial standard (N2.0 CO_2, 99%).

After full saturation in the equimolar DCB experiment, temperature-programmed desorption measurement was conducted at 60 °C (Figure S22). The desorption profiles revealed complete adsorbent regeneration in <50 min under a He flow of 20 cm^3 min^{-1}, underscoring the low-energy footprint for IPM-101 regeneration. Also aligning with the distinct breakthrough retention-driven adsorption trends, the desorption trends suggest significantly higher C_2H_2 desorbed versus CO_2. These results highlight that the adsorptive selectivity of IPM-101 toward C_2H_2 places it among a handful of sorbents which exhibit trace C_2H_2 removal from C_2H_2/CO_2 mixtures.[60,61]

Sorbent recyclability is needed to evaluate practical viability for swing experiments such as pressure swing, temperature swing, or pressure−temperature swing. Recycling studies performed with pure C_2H_2 revealed consistent performance across 10 consecutive adsorption−desorption cycles with an average kinetic uptake of ∼2.5 mmol g^{-1} (∼98% of the equilibrium C_2H_2 saturation capacity) (Figure 3c). Desorption kinetics suggested >99% removal of the adsorbed C_2H_2 within ∼25 min under N_2 flow (Figure 3c). For clarity of Figure 3c, points recorded during the initial activation are omitted and the first points of C_2H_2 loading are considered to be the first data points in each adsorption cycle (details in the SI). Importantly, the recycling stability of IPM-101 was confirmed by PXRD patterns recorded before and after the foregoing recycling experiment (Figure S23).

To understand the C_2H_2 selectivity of IPM-101, the binding sites, and adsorption energies, periodic density functional

https://doi.org/10.1021/acs.chemmater.1c01723

theory (DFT) calculations were performed (see Computational Methods Section in the SI). The unit cell parameters of the geometry-optimized structure were in close agreement with the parent MOF (Table S7). DFT calculations revealed the energy-minimized sites for C_2H_2 and CO_2 in IPM-101 (Figures 4 and S28). Hydrogen bonding interactions were found

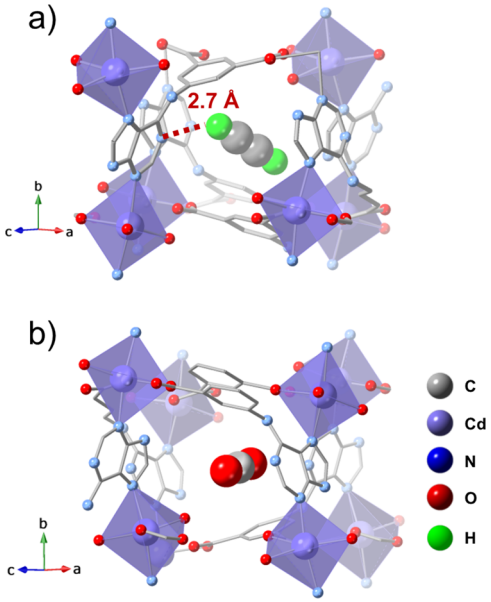

Figure 4. DFT-optimized guest-binding sites in IPM-101: (a) C_2H_2 and (b) CO_2; (a) also highlights the N···HC≡CH hydrogen bonding interaction between the framework N atoms and C_2H_2 molecules.

between a nitrogen atom of the purine moiety and C_2H_2 (N···HC≡CH) at a distance of 2.72 Å, while the corresponding bond angle between (N···HC) was determined as 144.04°. Interestingly, such interaction sites between the Lewis basic sites (O and N atoms) with the polar hydrogens of acetylene are well known.[63]

Conversely, for CO_2, no significant interaction site was found except for a weak van der Waals interaction between the oxygen atoms of CO_2 and the coordinated water molecule at the metal site. The latter interaction accounts for a significantly longer distance of 2.86 Å (Figure S28). It can thereby be inferred from this discussion that the strong interaction drives the high C_2H_2 affinity and excellent C_2H_2 capture performance. $Q_{st}(CO_2)$ and $Q_{st}(C_2H_2)$ adsorption enthalpies were determined by simulations to be ∼34.3 and 44.9 kJ mol^{-1}, respectively. These values are consistent with the experimental heats of adsorption, derived from Virial fits of C_2H_2 and CO_2 isotherms (Figure 2c). We also verified the adsorption enthalpies at four times higher loading (4 adsorbates per unit cell) and found that the average adsorption enthalpies stay within +/−0.5 kJ mol^{-1} of the calculated adsorption enthalpies at low loading. This is also in line with the experimental Q_{st} values, which are not affected by higher loading (Figure 2c). Overall, the theoretical studies complement the experimental results well and provide insights into the single binding site-based C_2H_2 selectivity.

3. CONCLUSIONS

In conclusion, we report gram-scale synthesis of a previously unreported ultramicroporous MOF, IPM-101, with one-dimensional ultramicropores that are lined by purine groups. A basic nitrogen atom of the purine ligand drives high affinity toward C_2H_2 compared to CO_2 and CH_4 with excellent C_2H_2 uptake registered even at a low pressure of ≤10 000 ppm. When compared to its negligible CO_2 and CH_4 uptakes, the result is high C_2H_2/CO_2 and C_2H_2/CH_4 selectivity and trace C_2H_2 removal. Overall, IPM-101 registers one of the highest separation selectivities among C_2H_2 selective physisorbents that can separate C_2H_2 from CO_2. A new record-high C_2H_2/CH_4 IAST selectivity is also set. Theoretical studies highlight the role of purine functionality in driving exceptionally high C_2H_2 selectivity by revealing the nature of the single binding site. This work exemplifies the untapped potential of tailored supramolecular design among MOF adsorbents in general, and reaffirms that the high density of tight binding sites that can exist in ultramicroporous MOFs can expedite efficiency in solid adsorbents for gas separation and purification.

4. EXPERIMENTAL SECTION

4.1. Synthesis of IPM-101. A mixture of ligand (14.9 mg, 0.05 mmol), $Cd(NO_3)\cdot 4H_2O$ (23.1 mg, 0.075 mmol), concentrated nitric acid (HNO_3) (10 μL), water (1 mL), and DMF (2 mL) was charged in a Teflon-capped vial, and this mixture was heated at 100 °C for 48 h and, thereafter, slowly cooled back to room temperature. Block-shaped single crystals were obtained at room temperature (yield ∼73%), and suitable crystals were selected for single-crystal X-ray diffraction analysis. Further, the bulk solid was separated by filtration and washed several times with DMF to remove any reactants. The vacuum-dried product (as-synthesized MOF) was further characterized by PXRD. To obtain the activated phase of IPM-101, this phase was soaked in low boiling acetonitrile (MeCN) for 3 days (MeCN replaced every 12 h), leading to the MeCN-exchanged phase. Evacuating the MeCN-exchanged phase at 110 °C for 12 h yielded the activated phase of IPM-101. CHN analysis: calculated C/H ratio (12.72), C/N (2.28); found C/H (12.57), C/N (2.18).

4.2. Gram-Scale Synthesis of IPM-101. The same protocol was followed for gram-scale synthesis as mentioned previously; however, the reactants were multiplied by 50 times in a 250 mL Teflon-capped vial; yield ∼ 76% with respect to the ligand.

4.3. Breakthrough Experiments. In typical breakthrough experiments, ∼0.5 g of preactivated IPM-101 sample was placed in quartz tubing (8 mm diameter; 8 × 6 × 400 mm^3) to form fixed beds. First, the adsorbent bed was purged under a 30 cm^3 min^{-1} flow of He gas at 383 K for 30 min prior to the breakthrough experiment. Upon cooling to room temperature, the gas flow was switched to the desired C_2H_2/CO_2 gas mixture compositions (1:1 and 1:99, respectively), maintained at a total flow rate of 1 cm^3 min^{-1}. Herein, 1:1 and 1:99 C_2H_2/CO_2 binary breakthrough experiments were conducted at 298 K for IPM-101 compound. The outlet composition was continuously monitored by a Shimadzu Nexis GC-2030 gas chromatograph until complete breakthrough was achieved. Dead volume was measured by replacing the column with a zero dead-volume connector and then passing injected helium to eventually multiply the elution time (measured between the moment of injection and the helium peak height) with the flow rate.

4.4. Adsorption Energy Calculations. A virial-type expression of the below form was used to fit the combined 273 and 298 K isotherm data of C_2H_2, CO_2, and CH_4 for IPM-101, where P is the pressure described in Pa, N is the adsorbed amount in mmol g^{-1}, T is the temperature in K, a_i and b_i are virial coefficients, and m and n are the number of coefficients used to describe the isotherms. Q_{st} is the coverage-dependent enthalpy of adsorption and R is the universal gas constant. All fitting was performed using Origin Pro 2016 (Origin(Pro), Version 2021, OriginLab Corporation, Northampton, MA, USA, licensed with Technical University of Munich). Fitting parameters thus obtained for IPM-101 can be found in Table S5 and Figures S24−S26.

https://doi.org/10.1021/acs.chemmater.1c01723

$$\ln P = \ln N + \sum_{i=0}^{m} a_i N_i + \sum_{i=0}^{n} \binom{n}{k} b_i N_i$$

Q_{st} was calculated from the virial model using the equation below

$$-Q_{st} = -R \sum_{i=0}^{m} a_i N_i$$

4.5. Adsorption Selectivity Calculations. The selectivities for the adsorbate mixture composition of interest were calculated from the single-component adsorption isotherms using Ideal Adsorbed Solution Theory (IAST), using a modified version of the program pyIAST.[75] First, the single-component isotherms for the gas sorbates at 298 K were fitted to the dual-site Langmuir–Freundlich (DSLF) equation

$$n(p) = \frac{q_1 (k_1 p)^{n_1}}{1 + (k_1 p)^{n_1}} + \frac{q_2 (k_2 p)^{n_2}}{1 + (k_2 p)^{n_2}}$$

In this equation, q_i is the amount adsorbed per unit mass of material (in $cm^3\ g^{-1}$), P is the total pressure (in torr) of the bulk gas at equilibrium with the adsorbed phase, q_1 and q_2 are the saturation uptakes (in $cm^3\ g^{-1}$) for sites 1 and 2, respectively, k_1 and k_2 are the affinity coefficients (in $torr^{-1}$) for sites 1 and 2, respectively, and ${n_1}^{-1}$ and ${n_2}^{-1}$ represent the deviations from the ideal homogeneous surface (unitless) for sites 1 and 2, respectively. The final selectivity for adsorbate i relative to adsorbate j was calculated using the following equation

$$s_i/j = \frac{x_i/x_j}{y_i/y_j}$$

Here, x_i and x_j are the mole fractions of components i and j, respectively, in the adsorbed phase and y_i and y_j are the mole fractions of components i and j, respectively, in the gas phase. Table S6 includes the DSLF fitting parameters.

4.6. Separation Selectivity Calculations. The amount of adsorbed gas i (q_i) is calculated from the breakthrough curve as follows

$$q_i = \frac{V_i T_0 - V_{dead} - \int_0^{t_0} V_e \Delta T}{m}$$

Here, V_i is the influent flow rate of gas ($cm^3\ min^{-1}$), V_e is the effluent flow rate of gas ($cm^3\ min^{-1}$), V_{dead} is the dead volume of the system (cm^3), T_0 is the adsorption time (min), and m is the mass of the sorbent (g).[76]

The separation factor, also known as separation selectivity (α) for the breakthrough experiment, i.e., breakthrough-derived selectivity, is determined as follows

$$\alpha = \frac{q_{1\,y_2}}{q_{2\,y_1}}$$

where y_i is the partial pressure of gas i in the gas mixture. In the case where one gas component has negligible adsorption, the amount of gas adsorbed is treated as $\leq 1\ cm^3$ for calculations.

For C_2H_2/CO_2 DCB experiments, the C_2H_2 concentration is defined by

$$\text{concentration}(C_2H_2) = \frac{\text{signal}(C_2H_2)}{\text{signal}(C_2H_2) + \text{signal}(CO_2)} \quad (1)$$

and CO_2 purity is defined by

$$\text{purity}(CO_2) = \frac{\text{signal}(CO_2)}{\text{signal}(C_2H_2) + \text{signal}(CO_2)} \quad (2)$$

The C_2H_2 uptake in the breakthrough experiment is defined by

$$n(C_2H_2) = \frac{\int_0^{t_2} (u_i y_{C_2H_2} - u_e(t) y_e(t) A dt}{V_m} = \frac{F \times y_{C_2H_2} \times \int_0^{t_2} (1 - \frac{C(t)}{C_0}) dt}{V_m} = \frac{F \times y_{C_2H_2} \times (t_2 - \int_0^{t_2} \frac{C(t)}{C_0} dt)}{V_m} \quad (3)$$

where n is the C_2H_2 uptake in mmol g^{-1}, t_2 is the C_2H_2 saturation time, $u_e(t)$ is the transient linear velocity in the outlet gas, $y_e(t)$ is the transient C_2H_2 volume fraction in the outlet gas, u_i is the transient linear velocity in the inlet gas, F is the inlet gas volume flow rate, $y_{C_2H_2}$ is the volume fraction of C_2H_2 in the mixed gas, $\int_0^{t_2} \frac{C(t)}{C_0} dt$ is the integrated area between the C_2H_2 breakthrough curve and the X-axis within the range 0 and t_2, $C(t)$ is the detected C_2H_2 concentration in the outlet gas, C_0 is the detected C_2H_2 concentration in the outlet gas, and V_m is the molar volume of the gas.

■ ASSOCIATED CONTENT

Supporting Information

The Supporting Information is available free of charge at https://pubs.acs.org/doi/10.1021/acs.chemmater.1c01723.

Materials and Methods—Ligand synthesis, physical measurements, X-ray structural studies, gas-sorption measurements, single-gas-sorption cycling test method, computational methods; supplementary Data—NMR data, crystal structure figures and topological analysis, PXRD patterns, TGA profile, FESEM images and elemental mapping, FT-IR, and single-component adsorption plots; comparative sorption plots, Q_{st} profiles, adsorption kinetics data, IAST selectivity trends, temperature-programmed desorption plot, post-adsorption PXRD patterns, virial fitting plots, schematic of breakthrough instrument setup, DFT-optimized geometries, crystal data, tabulated C_2H_2 and CO_2 sorption data, a comparison of sorption parameters of IPM-101 for C_2H_2/CO_2 separation with the literature; adsorption information files for the C_2H_2 and CO_2 isotherms recorded at 273 and 298 K[77,78] (PDF)

IPM-101 (CIF)

C_2H_2 modelled in IPM-101 (XYZ)

CO_2 modelled in IPM-101 (XYZ)

■ AUTHOR INFORMATION

Corresponding Authors

Michael J. Zaworotko − *Department of Chemical Sciences, Bernal Institute, University of Limerick, Limerick V94 T9PX, Republic of Ireland;* orcid.org/0000-0002-1360-540X; Email: xtal@ul.ie

Sujit K. Ghosh − *Department of Chemistry, Indian Institute of Science Education and Research, Pune 411008, India;* orcid.org/0000-0002-1672-4009; Email: sghosh@iiserpune.ac.in

Authors

Shivani Sharma − *Department of Chemistry, Indian Institute of Science Education and Research, Pune 411008, India*

Soumya Mukherjee − *Department of Chemical Sciences, Bernal Institute, University of Limerick, Limerick V94 T9PX, Republic of Ireland; Catalysis Research Center, Ernst-Otto-Fischer Straße 1 and Department of Chemistry, Technical*

https://doi.org/10.1021/acs.chemmater.1c01723

University of Munich, 85748 Garching bei München, Germany; orcid.org/0000-0003-2375-7009

Aamod V. Desai − *Department of Chemistry, Indian Institute of Science Education and Research, Pune 411008, India;* orcid.org/0000-0001-7219-3428

Matthias Vandichel − *Department of Chemical Sciences, Bernal Institute, University of Limerick, Limerick V94 T9PX, Republic of Ireland;* orcid.org/0000-0003-1592-0726

Gourab K. Dam − *Department of Chemistry, Indian Institute of Science Education and Research, Pune 411008, India*

Ashwini Jadhav − *Department of Chemistry, Indian Institute of Science Education and Research, Pune 411008, India*

Gabriele Kociok-Köhn − *Material and Chemical Characterization Facility (MC2), University of Bath, Bath BA2 7AY, U.K.;* orcid.org/0000-0002-7186-1399

Complete contact information is available at: https://pubs.acs.org/10.1021/acs.chemmater.1c01723

Author Contributions

[⊥]S.S. and S.M. contributed equally. The manuscript was written through contributions of all authors. All authors have given approval to the final version of the manuscript.

Notes

The authors declare no competing financial interest.

■ ACKNOWLEDGMENTS

S.S. and G.K.D. acknowledge the Council of Scientific and Industrial Research (CSIR) for fellowship. A.V.D. and A.J. thank IISER Pune for funding. S.M. acknowledges the Alexander von Humboldt foundation for postdoctoral research fellowship. G.K.K. thanks the University of Bath. M.V. acknowledges the Irish Centre for High-End Computing (ICHEC) for the provision of computational facilities and support. M.J.Z. acknowledges the Science Foundation Ireland (awards 13/RP/B2549 and 16/IA/4624) and the European Research Council under the European Union's H2020 research and innovation programme (grant agreement ADG 885695). S.K.G. thanks the SERB India for project funding (Grant No. CRG/2019/000906).

■ REFERENCES

(1) Sholl, D. S.; Lively, R. P. *Nature* **2016**, *532*, 6−9.

(2) Fan, W.; Yuan, S.; Wang, W.; Feng, L.; Liu, X.; Zhang, X.; Wang, X.; Kang, Z.; Dai, F.; Yuan, D.; Sun, D.; Zhou, H.-C. Optimizing Multivariate Metal−Organic Frameworks for Efficient C_2H_2/CO_2 Separation. *J. Am. Chem. Soc.* **2020**, *142*, 8728−8737.

(3) Matsuda, R.; Kitaura, R.; Kitagawa, S.; Kubota, Y.; Belosludov, R. V.; Kobayashi, T. C.; Sakamoto, H.; Chiba, T.; Takata, M.; Kawazoe, Y.; Mita, Y. Highly Controlled Acetylene Accommodation in a Metal-Organic Microporous Material. *Nature* **2005**, *436*, 238−241.

(4) Wang, T.; Lin, E.; Peng, Y.-L.; Chen, Y.; Cheng, P.; Zhang, Z. Rational Design and Synthesis of Ultramicroporous Metal-Organic Frameworks for Gas Separation. *Coord. Chem. Rev.* **2020**, *423*, No. 213485.

(5) Chen, K. J.; Scott, H. S.; Madden, D. G.; Pham, T.; Kumar, A.; Bajpai, A.; Lusi, M.; Forrest, K. A.; Space, B.; Perry, J. J.; Zaworotko, M. J. Benchmark C_2H_2/CO_2 and CO_2/C_2H_2 Separation by Two Closely Related Hybrid Ultramicroporous Materials. *Chem* **2016**, *1*, 753−765.

(6) Chrysalis Scientific Technologies Inc. http://www.chrysalisscientific.com/pg443-Lower-LEL-Upper-UEL-Explosive-Limits.pdf (accessed 2021-06-07).

(7) Cui, W.; Hu, T.; Bu, X. Metal−Organic Framework Materials for the Separation and Purification of Light Hydrocarbons. *Adv. Mater.* **2020**, *32*, No. 1806445.

(8) Kitagawa, S. Porous Materials and the Age of Gas. *Angew. Chem., Int. Ed.* **2015**, *54*, 10686−10687.

(9) Ji, Z.; Wang, H.; Canossa, S.; Wuttke, S.; Yaghi, O. M. Pore Chemistry of Metal−Organic Frameworks. *Adv. Funct. Mater.* **2020**, *30*, No. 2000238.

(10) Kitagawa, S.; Kitaura, R.; Noro, S. Functional Porous Coordination Polymers. *Angew. Chem., Int. Ed.* **2004**, *43*, 2334−2375.

(11) Lustig, W. P.; Mukherjee, S.; Rudd, N. D.; Desai, A. V.; Li, J.; Ghosh, S. K. Metal−Organic Frameworks: Functional Luminescent and Photonic Materials for Sensing Applications. *Chem. Soc. Rev.* **2017**, *46*, 3242−3285.

(12) Li, H.-Y.; Zhao, S.-N.; Zang, S.-Q.; Li, J. Functional Metal−Organic Frameworks as Effective Sensors of Gases and Volatile Compounds. *Chem. Soc. Rev.* **2020**, *49*, 6364−6401.

(13) Gu, C.; Hosono, N.; Zheng, J.-J.; Sato, Y.; Kusaka, S.; Sakaki, S.; Kitagawa, S. Design and Control of Gas Diffusion Process in a Nanoporous Soft Crystal. *Science* **2019**, *363*, 387−391.

(14) Karmakar, A.; Samanta, P.; Desai, A. V.; Ghosh, S. K. Guest-Responsive Metal-Organic Frameworks as Scaffolds for Separation and Sensing Applications. *Acc. Chem. Res.* **2017**, *50*, 2457−2469.

(15) Mukherjee, S.; Desai, A. V.; Ghosh, S. K. Potential of Metal−Organic Frameworks for Adsorptive Separation of Industrially and Environmentally Relevant Liquid Mixtures. *Coord. Chem. Rev.* **2018**, *367*, 82−126.

(16) Trickett, C. A.; Osborn Popp, T. M.; Su, J.; Yan, C.; Weisberg, J.; Huq, A.; Urban, P.; Jiang, J.; Kalmutzki, M. J.; Liu, Q.; Baek, J.; Head-Gordon, M. P.; Somorjai, G. A.; Reimer, J. A.; Yaghi, O. M. Identification of the Strong Brønsted Acid Site in a Metal−Organic Framework Solid Acid Catalyst. *Nat. Chem.* **2019**, *11*, 170−176.

(17) Otake, K. I.; Ye, J.; Mandal, M.; Islamoglu, T.; Buru, C. T.; Hupp, J. T.; Delferro, M.; Truhlar, D. G.; Cramer, C. J.; Farha, O. K. Enhanced Activity of Heterogeneous Pd(II) Catalysts on Acid-Functionalized Metal-Organic Frameworks. *ACS Catal.* **2019**, *9*, 5383−5390.

(18) Sharma, S.; Desai, A. V.; Joarder, B.; Ghosh, S. K. A Water-Stable Ionic MOF for the Selective Capture of Toxic Oxoanions of Se VI and As V and Crystallographic Insight into the Ion-Exchange Mechanism. *Angew. Chem., Int. Ed.* **2020**, *59*, 7788−7792.

(19) Islamoglu, T.; Chen, Z.; Wasson, M. C.; Buru, C. T.; Kirlikovali, K. O.; Afrin, U.; Mian, M. R.; Farha, O. K. Metal−Organic Frameworks against Toxic Chemicals. *Chem. Rev.* **2020**, *120*, 8130−8160.

(20) Xie, L. S.; Skorupskii, G.; Dincă, M. Electrically Conductive Metal−Organic Frameworks. *Chem. Rev.* **2020**, *120*, 8536−8580.

(21) Kung, C.-W.; Goswami, S.; Hod, I.; Wang, T. C.; Duan, J.; Farha, O. K.; Hupp, J. T. Charge Transport in Zirconium-Based Metal−Organic Frameworks. *Acc. Chem. Res.* **2020**, *53*, 1187−1195.

(22) Aubrey, M. L.; Wiers, B. M.; Andrews, S. C.; Sakurai, T.; Reyes-Lillo, S. E.; Hamed, S. M.; Yu, C. J.; Darago, L. E.; Mason, J. A.; Baeg, J. O.; Grandjean, F.; Long, G. J.; Seki, S.; Neaton, J. B.; Yang, P.; Long, J. R. Electron Delocalization and Charge Mobility as a Function of Reduction in a Metal-Organic Framework. *Nat. Mater.* **2018**, *17*, 625−632.

(23) Furukawa, H.; Cordova, K. E.; O'Keeffe, M.; Yaghi, O. M. The Chemistry and Applications of Metal-Organic Frameworks. *Science.* **2013**, *341*, No. 1230444.

(24) Feng, L.; Wang, K. Y.; Willman, J.; Zhou, H. C. Hierarchy in Metal-Organic Frameworks. *ACS Cent. Sci.* **2020**, *6*, 359−367.

(25) Slater, A. G.; Cooper, A. I. Function-Led Design of New Porous Materials. *Science* **2015**, *348*, No. aaa8075.

(26) Chen, K. J.; Madden, D. G.; Mukherjee, S.; Pham, T.; Forrest, K. A.; Kumar, A.; Space, B.; Kong, J.; Zhang, Q. Y.; Zaworotko, M. J. Synergistic Sorbent Separation for One-Step Ethylene Purification from a Four-Component Mixture. *Science* **2019**, *366*, 241−246.

(27) Bloch, E. D.; Queen, W. L.; Krishna, R.; Zadrozny, J. M.; Brown, C. M.; Long, J. R. Hydrocarbon Separations in a Metal-

Organic Framework with Open Iron(II) Coordination Sites. *Science* **2012**, *335*, 1606−1610.
(28) Mukherjee, S.; Zaworotko, M. J. Crystal Engineering of Hybrid Coordination Networks: From Form to Function. *Trends Chem.* **2020**, *2*, 506−518.
(29) Lama, P.; Aggarwal, H.; Bezuidenhout, C. X.; Barbour, L. J. Giant Hysteretic Sorption of CO_2: In Situ Crystallographic Visualization of Guest Binding within a Breathing Framework at 298 K. *Angew. Chem., Int. Ed.* **2016**, *55*, 13271−13275.
(30) Bhatt, P. M.; Belmabkhout, Y.; Cadiau, A.; Adil, K.; Shekhah, O.; Shkurenko, A.; Barbour, L. J.; Eddaoudi, M. A Fine-Tuned Fluorinated MOF Addresses the Needs for Trace CO2 Removal and Air Capture Using Physisorption. *J. Am. Chem. Soc.* **2016**, *138*, 9301−9307.
(31) McDonald, T. M.; Mason, J. A.; Kong, X.; Bloch, E. D.; Gygi, D.; Dani, A.; Crocellà, V.; Giordanino, F.; Odoh, S. O.; Drisdell, W. S.; Vlaisavljevich, B.; Dzubak, A. L.; Poloni, R.; Schnell, S. K.; Planas, N.; Lee, K.; Pascal, T.; Wan, L. F.; Prendergast, D.; Neaton, J. B.; Smit, B.; Kortright, J. B.; Gagliardi, L.; Bordiga, S.; Reimer, J. A.; Long, J. R. Cooperative Insertion of CO_2 in Diamine-Appended Metal-Organic Frameworks. *Nature* **2015**, *519*, 303−308.
(32) Nugent, P.; Giannopoulou, E. G.; Burd, S. D.; Elemento, O.; Giannopoulou, E. G.; Forrest, K.; Pham, T.; Ma, S.; Space, B.; Wojtas, L.; Eddaoudi, M.; Zaworotko, M. J. Porous Materials with Optimal Adsorption Thermodynamics and Kinetics for CO_2 Separation. *Nature* **2013**, *495*, 80−84.
(33) Mukherjee, S.; Chen, S.; Bezrukov, A. A.; Mostrom, M.; Terskikh, V. V.; Franz, D.; Wang, S.; Kumar, A.; Chen, M.; Space, B.; Huang, Y.; Zaworotko, M. J. Ultramicropore Engineering by Dehydration to Enable Molecular Sieving of H_2 by Calcium Trimesate. *Angew. Chem., Int. Ed.* **2020**, *59*, 16188−16194.
(34) Pei, J.; Shao, K.; Wang, J.; Wen, H.; Yang, Y.; Cui, Y.; Krishna, R.; Li, B.; Qian, G. A Chemically Stable Hofmann-Type Metal−Organic Framework with Sandwich-Like Binding Sites for Benchmark Acetylene Capture. *Adv. Mater.* **2020**, *32*, No. 1908275.
(35) Cui, X.; Chen, K.; Xing, H.; Yang, Q.; Krishna, R.; Bao, Z.; Wu, H.; Zhou, W.; Dong, X.; Han, Y.; Li, B.; Ren, Q.; Zaworotko, M. J.; Chen, B. Pore Chemistry and Size Control in Hybrid Porous Materials for Acetylene Capture from Ethylene. *Science* **2016**, *353*, 141−144.
(36) Zhang, Y.; Li, B.; Krishna, R.; Wu, Z.; Ma, D.; Shi, Z.; Pham, T.; Forrest, K.; Space, B.; Ma, S. Highly Selective Adsorption of Ethylene over Ethane in a MOF Featuring the Combination of Open Metal Site and π-Complexation. *Chem. Commun.* **2015**, *51*, 2714−2717.
(37) Qazvini, O. T.; Babarao, R.; Shi, Z.-L.; Zhang, Y.-B.; Telfer, S. G. A Robust Ethane-Trapping Metal−Organic Framework with a High Capacity for Ethylene Purification. *J. Am. Chem. Soc.* **2019**, *141*, 5014−5020.
(38) Zhang, L.; Li, L.; Hu, E.; Yang, L.; Shao, K.; Yao, L.; Jiang, K.; Cui, Y.; Yang, Y.; Li, B.; Chen, B.; Qian, G. Boosting Ethylene/Ethane Separation within Copper(I)-Chelated Metal−Organic Frameworks through Tailor-Made Aperture and Specific π-Complexation. *Adv. Sci.* **2020**, *7*, No. 1901918.
(39) Liao, P. Q.; Zhang, W. X.; Zhang, J. P.; Chen, X. M. Efficient Purification of Ethene by an Ethane-Trapping Metal-Organic Framework. *Nat. Commun.* **2015**, *6*, No. 8697.
(40) Li, L.; Wen, H. M.; He, C.; Lin, R. B.; Krishna, R.; Wu, H.; Zhou, W.; Li, J.; Li, B.; Chen, B. A Metal−Organic Framework with Suitable Pore Size and Specific Functional Sites for the Removal of Trace Propyne from Propylene. *Angew. Chem., Int. Ed.* **2018**, *57*, 15183−15188.
(41) Cadiau, A.; Adil, K.; Bhatt, P. M.; Belmabkhout, Y.; Eddaoudi, M. A Metal-Organic Framework-Based Splitter for Separating Propylene from Propane. *Science* **2016**, *353*, 137−140.
(42) Lee, J.; Chuah, C. Y.; Kim, J.; Kim, Y.; Ko, N.; Seo, Y.; Kim, K.; Bae, T. H.; Lee, E. Separation of Acetylene from Carbon Dioxide and Ethylene by a Water-Stable Microporous Metal−Organic Framework with Aligned Imidazolium Groups inside the Channels. *Angew. Chem., Int. Ed.* **2018**, *57*, 7869−7873.
(43) Lu, Z.; Godfrey, H. G. W.; Da Silva, I.; Cheng, Y.; Savage, M.; Manuel, P.; Rudić, S.; Ramirez-Cuesta, A. J.; Yang, S.; Schröder, M. Direct Observation of Supramolecular Binding of Light Hydrocarbons in Vanadium(III) and (IV) Metal-Organic Framework Materials. *Chem. Sci.* **2018**, *9*, 3401−3408.
(44) Lin, R. B.; Li, L.; Wu, H.; Arman, H.; Li, B.; Lin, R. G.; Zhou, W.; Chen, B. Optimized Separation of Acetylene from Carbon Dioxide and Ethylene in a Microporous Material. *J. Am. Chem. Soc.* **2017**, *139*, 8022−8028.
(45) Duan, J.; Higuchi, M.; Zheng, J.; Noro, S. I.; Chang, I. Y.; Hyeon-Deuk, K.; Mathew, S.; Kusaka, S.; Sivaniah, E.; Matsuda, R.; Sakaki, S.; Kitagawa, S. Density Gradation of Open Metal Sites in the Mesospace of Porous Coordination Polymers. *J. Am. Chem. Soc.* **2017**, *139*, 11576−11583.
(46) Luo, F.; Yan, C.; Dang, L.; Krishna, R.; Zhou, W.; Wu, H.; Dong, X.; Han, Y.; Hu, T. L.; O'Keeffe, M.; Wang, L.; Luo, M.; Lin, R. B.; Chen, B. UTSA-74: A MOF-74 Isomer with Two Accessible Binding Sites per Metal Center for Highly Selective Gas Separation. *J. Am. Chem. Soc.* **2016**, *138*, 5678−5684.
(47) Li, Y. P.; Wang, Y.; Xue, Y. Y.; Li, H. P.; Zhai, Q. G.; Li, S. N.; Jiang, Y. C.; Hu, M. C.; Bu, X. Ultramicroporous Building Units as a Path to Bi-Microporous Metal−Organic Frameworks with High Acetylene Storage and Separation Performance. *Angew. Chem., Int. Ed.* **2019**, *58*, 13590−13595.
(48) Peng, Y. L.; Pham, T.; Li, P.; Wang, T.; Chen, Y.; Chen, K. J.; Forrest, K. A.; Space, B.; Cheng, P.; Zaworotko, M. J.; Zhang, Z. Robust Ultramicroporous Metal−Organic Frameworks with Benchmark Affinity for Acetylene. *Angew. Chem., Int. Ed.* **2018**, *57*, 10971−10975.
(49) Moreau, F.; Da Silva, I.; Al Smail, N. H.; Easun, T. L.; Savage, M.; Godfrey, H. G. W.; Parker, S. F.; Manuel, P.; Yang, S.; Schröder, M. Unravelling Exceptional Acetylene and Carbon Dioxide Adsorption within a Tetra-Amide Functionalized Metal-Organic Framework. *Nat. Commun.* **2017**, *8*, No. 14085.
(50) Zeng, H.; Xie, M.; Huang, Y. L.; Zhao, Y.; Xie, X. J.; Bai, J. P.; Wan, M. Y.; Krishna, R.; Lu, W.; Li, D. Induced Fit of C_2H_2 in a Flexible MOF Through Cooperative Action of Open Metal Sites. *Angew. Chem., Int. Ed.* **2019**, *58*, 8515−8519.
(51) Yang, H.; Trieu, T. X.; Zhao, X.; Wang, Y.; Wang, Y.; Feng, P.; Bu, X. Lock-and-Key and Shape-Memory Effects in an Unconventional Synthetic Path to Magnesium Metal−Organic Frameworks. *Angew. Chem., Int. Ed.* **2019**, *58*, 11757−11762.
(52) Adil, K.; Belmabkhout, Y.; Pillai, R. S.; Cadiau, A.; Bhatt, P. M.; Assen, A. H.; Maurin, G.; Eddaoudi, M. Gas/Vapour Separation Using Ultra-Microporous Metal−Organic Frameworks: Insights into the Structure/Separation Relationship. *Chem. Soc. Rev.* **2017**, *46*, 3402−3430.
(53) Mukherjee, S.; Sensharma, D.; Chen, K. J.; Zaworotko, M. J. Crystal Engineering of Porous Coordination Networks to Enable Separation of C2 Hydrocarbons. *Chem. Commun.* **2020**, *56*, 10419−10441.
(54) Li, A.; Bueno-Perez, R.; Wiggin, S.; Fairen-Jimenez, D. Enabling Efficient Exploration of Metal−Organic Frameworks in the Cambridge Structural Database. *CrystEngComm* **2020**, *22*, 7152−7161.
(55) Fu, X.-P.; Wang, Y.-L.; Liu, Q.-Y. Metal−Organic Frameworks for C_2H_2/CO_2 Separation. *Dalton Trans.* **2020**, *49*, 16598−16607.
(56) Gu, Y.; Zheng, J.-J.; Otake, K.; Shivanna, M.; Sakaki, S.; Yoshino, H.; Ohba, M.; Kawaguchi, S.; Wang, Y.; Li, F.; Kitagawa, S. Host-guest Interaction Modulation in Porous Coordination Polymers for Inverse Selective CO_2/C_2H_2 Separation. *Angew. Chem., Int. Ed.* **2021**, *60*, 11688−11694.
(57) Foo, M. L.; Matsuda, R.; Hijikata, Y.; Krishna, R.; Sato, H.; Horike, S.; Hori, A.; Duan, J.; Sato, Y.; Kubota, Y.; Takata, M.; Kitagawa, S. An Adsorbate Discriminatory Gate Effect in a Flexible Porous Coordination Polymer for Selective Adsorption of CO_2 over C_2H_2. *J. Am. Chem. Soc.* **2016**, *138*, 3022−3030.

https://doi.org/10.1021/acs.chemmater.1c01723

(58) Qazvini, O. T.; Babarao, R.; Telfer, S. G. Selective Capture of Carbon Dioxide from Hydrocarbons Using a Metal-Organic Framework. *Nat. Commun.* **2021**, *12*, No. 197.
(59) Xie, Y.; Cui, H.; Wu, H.; Lin, R. B.; Zhou, W.; Chen, B. Electrostatically Driven Selective Adsorption of Carbon Dioxide over Acetylene in an Ultramicroporous Material. *Angew. Chem., Int. Ed.* **2021**, *60*, 9604−9609.
(60) Qazvini, O. T.; Babarao, R.; Telfer, S. G. Multipurpose Metal-Organic Framework for the Adsorption of Acetylene: Ethylene Purification and Carbon Dioxide Removal. *Chem. Mater.* **2019**, *31*, 4919−4926.
(61) Mukherjee, S.; He, Y.; Franz, D.; Wang, S. Q.; Xian, W. R.; Bezrukov, A. A.; Space, B.; Xu, Z.; He, J.; Zaworotko, M. J. Halogen−C_2H_2 Binding in Ultramicroporous Metal−Organic Frameworks (MOFs) for Benchmark C_2H_2/CO_2 Separation Selectivity. *Chem.−Eur. J.* **2020**, *26*, 4923−4929.
(62) Li, J.; Jiang, L.; Chen, S.; Kirchon, A.; Li, B.; Li, Y.; Zhou, H. C. Metal-Organic Framework Containing Planar Metal-Binding Sites: Efficiently and Cost-Effectively Enhancing the Kinetic Separation of C_2H_2/C_2H_4. *J. Am. Chem. Soc.* **2019**, *141*, 3807−3811.
(63) Zhang, Z.; Peh, S. B.; Wang, Y.; Kang, C.; Fan, W.; Zhao, D. Efficient Trapping of Trace Acetylene from Ethylene in an Ultramicroporous Metal−Organic Framework: Synergistic Effect of High-Density Open Metal and Electronegative Sites. *Angew. Chem., Int. Ed.* **2020**, *59*, 18927−18932.
(64) Spek, A. L. Single-Crystal Structure Validation with the Program PLATON. *J. Appl. Crystallogr.* **2003**, *36*, 7−13.
(65) Wang, J.; Zhang, Y.; Zhang, P.; Hu, J.; Lin, R.; Deng, Q.; Zeng, Z.; Xing, H.; Deng, S.; Chen, B. Optimizing Pore Space for Flexible-Robust Metal − Organic Framework to Boost Trace Acetylene Removal. *J. Am. Chem. Soc.* **2020**, *142*, 9744−9751.
(66) Rouquerol, J.; Rouquerol, F.; Llewellyn, P.; Maurin, G.; Sing, K. S. W. *Adsorption by Powders and Porous Solids*; Elsevier, 2014.
(67) Gao, J.; Qian, X.; Lin, R.; Krishna, R.; Wu, H.; Zhou, W.; Chen, B. Mixed Metal−Organic Framework with Multiple Binding Sites for Efficient C_2H_2/CO_2 Separation. *Angew. Chem.* **2020**, *132*, 4426−4430.
(68) Scott, H. S.; Shivanna, M.; Bajpai, A.; Madden, D. G.; Chen, K. J.; Pham, T.; Forrest, K. A.; Hogan, A.; Space, B.; Iv, J. J. P.; Zaworotko, M. J. Highly Selective Separation of C_2H_2 from CO_2 by a New Dichromate-Based Hybrid Ultramicroporous Material. *ACS Appl. Mater. Interfaces* **2017**, *9*, 33395−33400.
(69) Li, B.; Cui, X.; O'Nolan, D.; Wen, H.-M.; Jiang, M.; Krishna, R.; Wu, H.; Lin, R.-B.; Chen, Y.-S.; Yuan, D.; Xing, H.; Zhou, W.; Ren, Q.; Qian, G.; Zaworotko, M. J.; Chen, B. An Ideal Molecular Sieve for Acetylene Removal from Ethylene with Record Selectivity and Productivity. *Adv. Mater.* **2017**, *29*, No. 1704210.
(70) Oschatz, M.; Antonietti, M. A Search for Selectivity to Enable CO_2 Capture with Porous Adsorbents. *Energy Environ. Sci.* **2018**, *11*, 57−70.
(71) Zhang, L.; Cui, X.; Xing, H.; Yang, Y.; Cui, Y.; Chen, B.; Qian, G. An Amino-Coordination Metal-Organic Framework for Highly Selective C_2H_2/CH_4 and C_2H_2/C_2H_4 Separations through the Appropriate Control of Window Sizes. *RSC Adv.* **2017**, *7*, 20795−20800.
(72) Duan, X.; Zhang, Q.; Cai, J.; Yang, Y.; Cui, Y.; He, Y.; Wu, C.; Krishna, R.; Chen, B.; Qian, G. A New Metal-Organic Framework with Potential for Adsorptive Separation of Methane from Carbon Dioxide, Acetylene, Ethylene, and Ethane Established by Simulated Breakthrough Experiments. *J. Mater. Chem. A* **2014**, *2*, 2628−2633.
(73) Li, P.; He, Y.; Zhao, Y.; Weng, L.; Wang, H.; Krishna, R.; Wu, H.; Zhou, W.; O'Keeffe, M.; Han, Y.; Chen, B. A Rod-Packing Microporous Hydrogen-Bonded Organic Framework for Highly Selective Separation of C_2H_2/CO_2 at Room Temperature. *Angew. Chem., Int. Ed.* **2015**, *54*, 574−577.
(74) Kumar, N.; Mukherjee, S.; Bezrukov, A. A.; Vandichel, M.; Shivanna, M.; Sensharma, D.; Bajpai, A.; Gascón, V.; Otake, K.; Kitagawa, S.; Zaworotko, M. J. A Square Lattice Topology Coordination Network That Exhibits Highly Selective C_2H_2/CO_2 Separation Performance. *SmartMat* **2020**, *1*, No. e1008.
(75) Myers, A. L.; Prausnitz, J. M. Thermodynamics of Mixed-gas Adsorption. *AIChE J.* **1965**, *11*, 121−127.
(76) Mukherjee, S.; He, Y.; Franz, D.; Wang, S. Q.; Xian, W. R.; Bezrukov, A. A.; Space, B.; Xu, Z.; He, J.; Zaworotko, M. J. Halogen−C_2H_2 Binding in Ultramicroporous Metal−Organic Frameworks (MOFs) for Benchmark C_2H_2/CO_2 Separation Selectivity. *Chem. - Eur. J.* **2020**, *26*, 4923−4929.
(77) Evans, J. D.; Bon, V.; Senkovska, I.; Kaskel, S. A Universal Standard Archive File for Adsorption Data. *Langmuir* **2021**, *37*, 4222−4226.
(78) Sharma, S.; Mukherjee, S.; Desai, A. V.; Vandichel, M.; Dam, G. K.; Jadhav, A.; Köhn, G. K.; Zaworotko, M. J.; Ghosh, S. K. Efficient capture of trace acetylene by an ultramicroporous metal-organic framework with purine binding sites *Zenodo* 2021, data set DOI: 10.5281/zenodo.4972093.

https://doi.org/10.1021/acs.chemmater.1c01723